SMARTPHONE ACOUSTIC IMPEDANCE SENSING BASED ON ADDITIVE SUM MIXING TECHNIQUE

BY

YUKUN REN

THESIS

Submitted in partial fulfillment of the requirements
for the degree of Master of Science in Electrical and Computer Engineering
in the Graduate College of the
University of Illinois at Urbana-Champaign, 2015

Urbana, Illinois

Advisor:

Associate Professor Logan Liu

ABSTRACT

We have developed a method to perform impedance measurement using general purpose smartphones that will not require the presence of external power source. The need for battery-less impedance sensing methods is greatly demanded given recent years' advancements in impedance based sensing technologies, such as impedance tomography, which will enable patients to perform medical tests such as breast cancer self-detection using only a smartphone.

The work discussed in this thesis is an early prototype of the impedance sensing method done using MATLAB simulation of both hardware and algorithm for impedance sensing. The battery-less acoustic impedance sensing technique is a combination of both hardware circuit design as well as control software algorithm. The circuit hardware technology is based on the additive summing mixer technology that is widely used in professional audio production mixing consoles. The results presented in this thesis can be accurate to within 0.1% of target device characteristics in simulation as far as tested.

Although not discussed in this work, in our early physical hardware prototypes, the measurement based on the method discussed in this thesis has achieved accuracy within 10% of the target value with all the noise and parameter approximations.

ACKNOWLEDGEMENTS

I would like to deliver my sincere gratitude to my master's adviser, Professor Gang Logan Liu, for providing me with the opportunity to pursue my master's degree in UIUC.

In addition, I would love to acknowledge my fellow group members in the Liu Nanobionics Lab as well as the staff members working in the ECE Electronics Service shop for their patience and generous guidance.

Finally, I thank my family for all the love and patience along the way.

TABLE OF CONTENTS

CHAPTER 1:

INTRODUCTION

1.1 Impedance Measurement History and Motivation

According to [1], "Electrical impedance is the measure of the opposition that a circuit presents to a current when a voltage is applied." The phenomenon of impedance was first documented by Oliver Heaviside in [2]. Because impedance is a phenomenon caused by a certain material's reaction to an applied voltage, scientists have since been utilizing impedance to characterize material properties. This thesis will focus on the applications of impedance measurements in the field of biomedical diagnostics.

The alternating current (AC) electrical measurement in the field of biomedical diagnostics was first implemented by [3]. In Schwan's research, by applying AC voltages under variable frequencies and observing the resulting impedance characteristics of the material under test, the technique of impedance spectroscopy was created in the process. Schwan is also known as the father of modern bioengineering for his research in electrical characterizations of body tissues and impedance plethysmography. The technique of impedance plethysmography has since been applied in many applications for health monitoring. [4] shows one example of the uses of the impedance plethysmography technique to detect congestive heart failure in its early stages, thus preventing more catastrophic consequences when the disease progresses into later and more serious stages.

Given the advancement in the portable computing and wearable devices markets, it is viable to apply the technique of impedance plethysmography to monitor various human health metrics using portable and wearable devices. The heath tracking devices currently available on the market can only track very basic health metrics such as heart rate and steps taken. Heart rate is measured using the technique of photoplethysmogram (PPG), which estimates the skin blood flow using infrared light [5]. In a photoplethysmography, an optical signal generator shines a light into the skin and the refracted signal is extracted by a detector. PPG works very well for detecting heart beats since the responding signal's peaks are easily distinguishable; hence "Traditionally, it measures the oxygen saturation, blood pressure, cardiac output, and for assessing autonomic functions" [5]; however, the performance of the photoplethysmogram can be affected by many factors including skin color, moisture level and the presence of hair. Also, the photoplethysmogram is limited to measuring only heart rate and blood oxygen level due to its non-constant DC offset and peak amplitude offset. According to [6], "In general, this relationship can be easily confounded due to local changes in the microvasculature and therefore may be difficult to determine on a beat-to-beat basis."

To overcome the current measurement inaccuracies caused by the hardware limitations of photoplethysmogram, the technique of impedance plethysmography should be examined. This paper presents an acoustic impedance measuring technique based on the analog sum mixer technique borrowed from the field of audio engineering. The mixer implementations will be discussed in chapter 2.

1.2 Impedance Measurement Techniques

The basic representation of impedance is "generally defined as the total opposition a device or circuit offers to the flow of an alternating current (AC) at a given frequency, and is represented as a complex quantity which is graphically shown on a vector plane" [1]. Figure 1.1 shows an example of vector representation of a complex impedance.

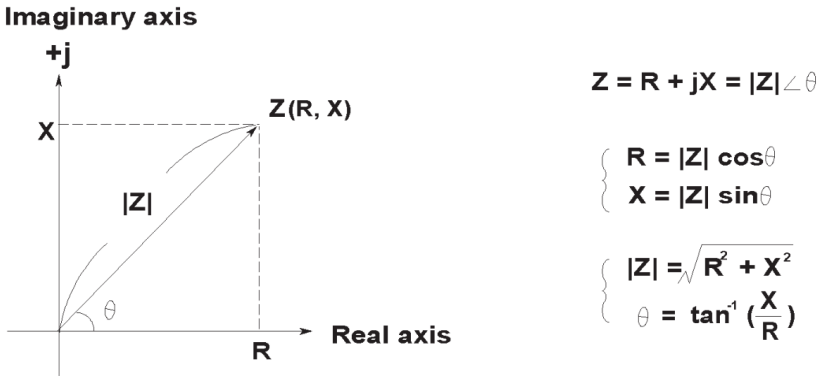

Figure 1.1: Complex impedance representations [7]

As shown in figure 1.1, impedance can be expressed using the complex expression in rectangular coordinate $R + jX$, where R is the resistance and X is the reactance. During impedance measurement, the polar coordinate expression $|Z| \angle \theta$ is more useful when it is necessary to extract amplitude attenuation and phase shift. It is sufficient to perform a basic circuit analysis on a basic RC filter circuit to show how the circuit produces a phase and amplitude shifted output signal from a pure tone sinusoidal input signal. Figure 1.2 shows an LPF circuit, and figure 1.3 shows the Spice simulation of the circuit's input and output voltage responses.

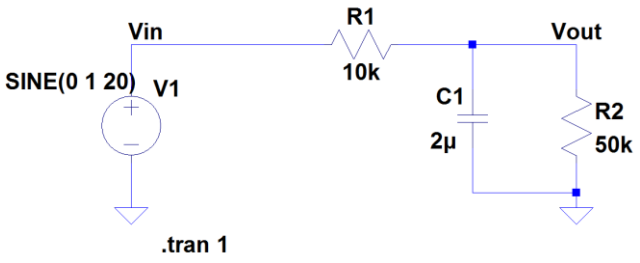

Figure 1.2: Low-pass circuit

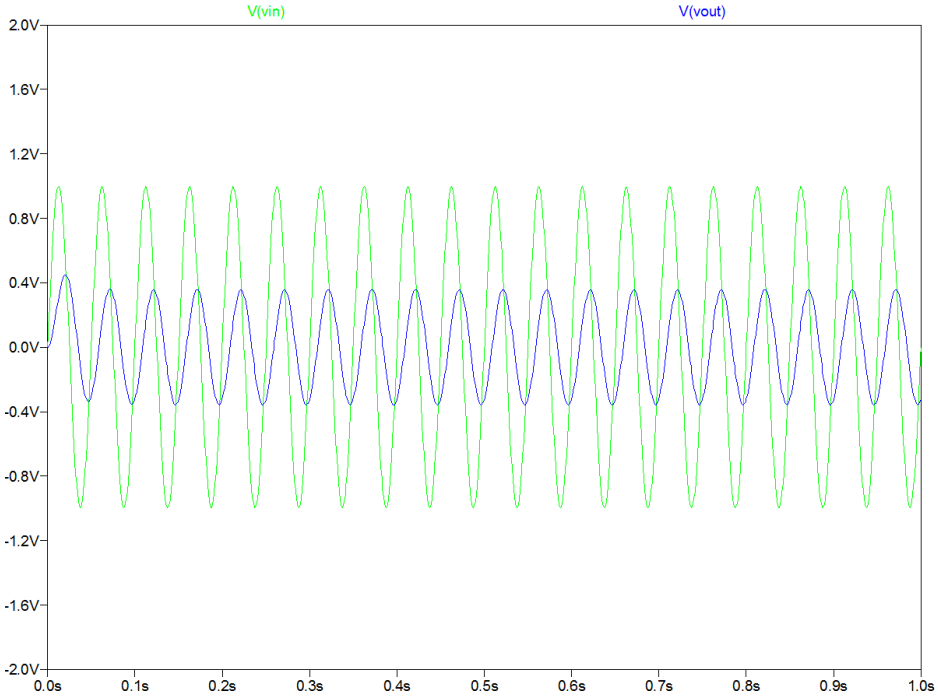

Figure 1.3: Transient analysis of input/output voltages of figure 1.2

To quantify the input and output voltage response of the circuit shown in figure 1.2 mathematically, Ohm's law can be applied. Although figure 1.2 is the most fundamental circuit example, using the amplitude and phase observations to characterize the system response can be applied to any circuit system. This basic principle lies behind most of the commercially available LCR meters as a part of the "auto-balancing bridge" circuit

structure shown in figure 1.4. By using the auto-balancing current flowing through both the DUT and ranging resistor R_r, the phase information is embedded in the calculations when dividing the input voltage V_x by the auto-balancing current I_r.

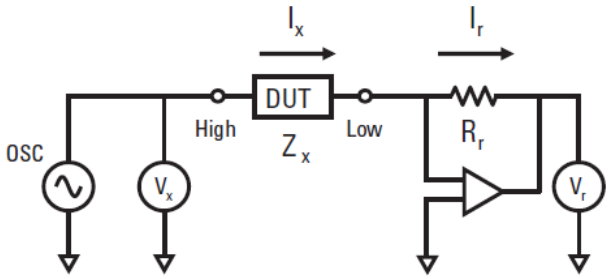

Figure 1.4: Auto-balancing bridge [7]

1.3 Commercial Network Analyzer IC: AD5933

The "auto-balancing bridge" method discussed in section 1.2 is the easiest and most reliable method of impedance measurement given the availability of signal conditioning hardware; however, provided the constraint of hardware for smartphone based sensing, the "auto-balancing bridge" technique is not suitable. Instead, a more brute-force phase measurement technique is needed. A commercial IC implementation by Analog Devices, the AD5933 is a widely used network analyzer IC used for impedance measurements. The functional block diagram of AD5933 is shown in figure 1.5.

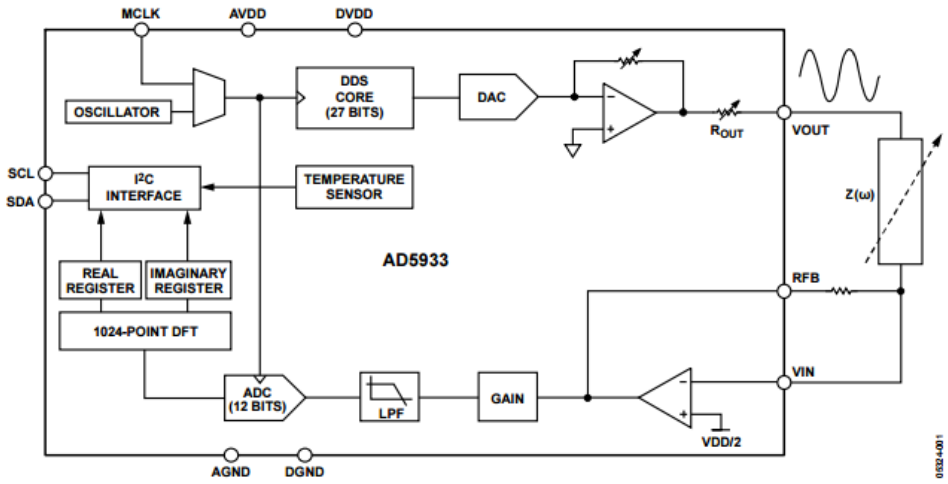

Figure 1.5: AD5933 functional block diagram [8]

The AD5933 measures the unknown Z(w) by exciting the external complex impedance with a known frequency. “The response signal from the impedance is sampled by the on-board ADC and DFT processed by an on-board DSP engine” [8]. The DSP process is described by equation 1.1.

$$X(f) = \sum_{n=0}^{1023} (x(n)(\cos(n) - j\sin(n))) \tag{1.1}$$

Through the point-to-point mapping of the cosine and sine test vectors, the chip can deduce amplitude and phase shift between the generated signal and the received signal. The phase comparison can be implemented easily on a real time system like the AD5933 because the software overhead is low and hardware physical placement can be precisely controlled. The performance of the AD5933 in the field is very good when power supply options are abundant; however, for the purpose of the proposed battery-less impedance sensing implementation, the power dependency makes the use of an external chip

infeasible although some successful demonstrations of energy harvesting have been done in the recent years. [9]

1.4 Stereo Soundcard RLC Measurement

Also using amplitude attenuation and phase shift to measure impedance, the method proposed by Klaper and Mathis [10] uses a stereo input/output sound card to perform the impedance measurement. The functional block diagram of method A presented in the paper is shown in figure 1.6.

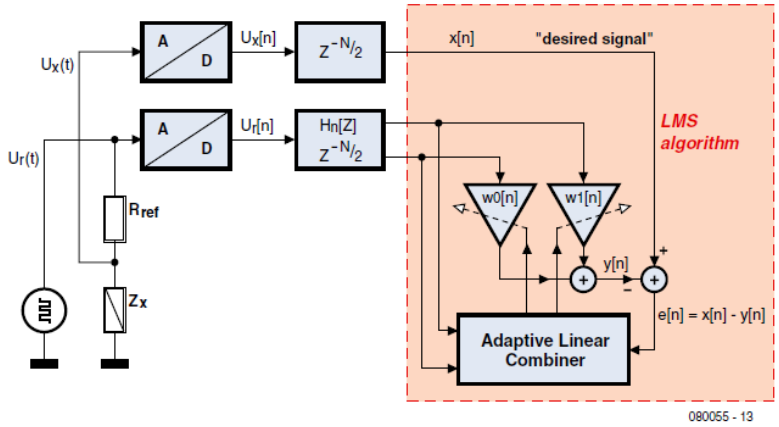

Figure 1.6: Soundcard impedance Measurement Method A [10]

The advantage of using a complete stereo generate and record system is the capability of comparing two branches in real time. As shown in figure 1.6, the method utilizes the classic LMS [11] adaptive filter architecture; by adjusting the weight coefficients *w* in incremental steps with each *w* term corresponding to the real and imaginary components of the impedance, the adaptive LMS algorithm will be able to find the optimum weight

coefficients which will bring the signal of interest closest to the reference signal. The detailed description of the algorithm can be found in Klaper and Mathis' original article [10].

1.5 Acoustic Summing Mixer-based Impedance Sensing

With a fully stereo input/output signal generation and recording system, it is easy to perform phase shift analysis in order to conduct impedance analysis as briefly discussed in section1.4; however, to implement a similar acoustic impedance sensing mechanism on general purpose smartphones is more involved. Modern day smartphones always provide a stereo audio output on the headphone jack for listening to music, but the microphone input channel is almost always mono (one channel) as this feature characteristic is standardized across all smartphone and headphone manufacturers.

This thesis presents a new impedance measurement method that can be used on general purpose handheld smartphone devices. The measurement principle behind the proposed measurement technique is the phase shift method used in all of the examples discussed in this chapter. By using the audio additive summing mixer circuit topology found on audio mixer consoles and signal reconstruction techniques, this thesis demonstrates a technique to overcome the limitations to performing impedance measurement found on general purpose smartphone devices.

CHAPTER 2:

THE ANALOG MIXER

To encode frequency information of two different frequencies, it is natural to use the electronic mixer technologies. The working principles of electronic mixers are purely based on mathematics and in the world of electronic mixers, there are mainly two types: product (multiplicative) and sum (additive) illustrated in figures 2.1 and 2.2, respectively. In this work, the additive mixer is used instead of the more popular multiplicative mixer. The choice is based on physical limitations of the smartphone platform as well as the algorithm; the differences between the two mixers will be discussed in sections 2.1 and 2.2.

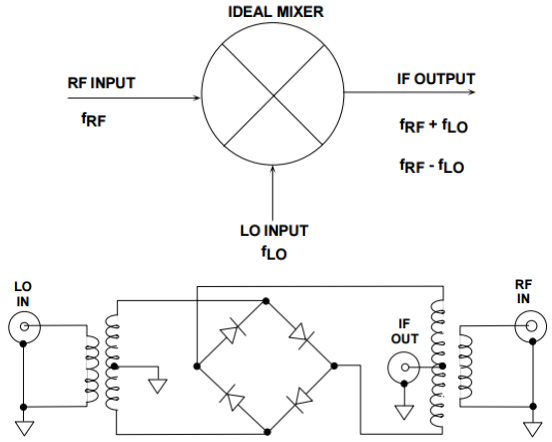

Figure 2.1: Multiplicative mixer [12]

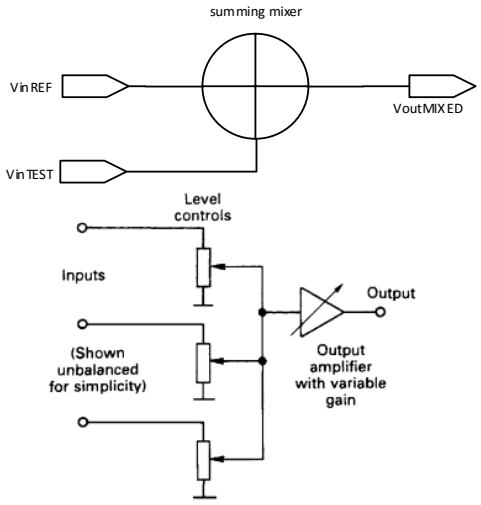

Figure 2.2: Additive mixer [13]

2.1 Multiplicative Diode Mixer

The multiplicative mixer shown in figure 2.1 is predominantly used in the RF world when high frequency information needs to be encoded in a lower frequency carrier signal such as AM and FM radio technologies. The mathematical model of the multiplicative mixer is simply the product of two pure tone sinusoidal signals as shown in equations 2.1 and 2.2:

$$V_o = [A_1 \cos(\omega_1 t)][A_2 \cos(\omega_2 t)] \tag{2.1}$$

$$V_o = \frac{A_1 A_2}{2}[\cos(\omega_1 - \omega_2)t + \cos(\omega_1 + \omega_2)t] \tag{2.2}$$

To use a multiplicative mixer, from a mathematical point, it is desirable to have signals with high amplitude to avoid signal attenuation due to the multiplication of amplitudes. To overcome the signal attenuation issues, in practice, most RF transmitter/receivers will have an RF amplifier before the filtering stages. However, in the battery-less smartphone acoustic sensing application, it is not feasible to amplify the weak audio signals without a DC power source. In addition to the weak output audio signals, mixing two channels multiplicatively, it often will require a diode mixing bridge. The presence of a pair of two diodes will further reduce the already small headroom of the audio signals by at least 300 mV if low forward drop Schottky diodes were to be used. Hence it is not reasonable to use a traditional multiplicative frequency mixer for the application presented in this paper despite the numerous advantages the multiplicative mixer has over the additive summing mixer.

2.2 Additive Summing Mixer

The additive summing mixer shown in figure 2.2 can be found in audio applications, mainly the audio mixing consoles used in production studios. Despite the recent advancements in digital audio mixing consoles, the professional studio-grade consoles are still mainly analog due to the superior audio signal fidelity that can be attained by the additive summing mixer architecture.

Comparing the performance of the additive summing mixer to that of multiplicative mixer as discussed in section 2.1, from the circuit's perspective as shown in figure 2.2, the use of a pure passive additive summing mixer will eliminate the need for the diode bridge, thus increasing the dynamic range of the sensing system, this feature also preserves the signal fidelity by eliminating the noise created by the diodes.

The mathematical derivation of the summing mixer is shown in equations 2.3 through 2.5. It is important to note that the derivation shown in equations 2.3 through 2.5 is only valid for two signals with the same amplitude magnitudes. If the two signals have different amplitudes, the resulting mixed output will contain a series of sums of the product shown in 2.5. The importance of matching the amplitudes of signals prior to mixing will be discussed in greater detail in chapters 2.3 and 2.4.

$$\sin(x) = \sin(2\pi f_1 t + \alpha), \sin(\mathrm{y}) = \sin(2\pi f_2 t + \beta) \tag{2.3}$$

$$\sin(x) + \sin(y) = 2\sin(\frac{x+y}{2})\cos(\frac{x-y}{2}) \tag{2.4}$$

$$V_{out,mixed} = 2\sin(\frac{2\pi(f_1+f_2)}{2}t+\frac{\alpha+\beta}{2})\cos(\frac{2\pi(f_1-f_2)}{2}t+\frac{\alpha-\beta}{2}) \qquad (2.5)$$

2.3 Mathematical Model Simulation

The mathematical expression shown in equation 2.5 is very similar to the multiplicative mixer's expression, which is simply the product of two sinusoidal signals. The significance of the additive summing mixer for the impedance sensing application is its ability to perform signal reconstruction based on input signal amplitude matching and phase matching.

As discussed in section 2.2, it is important for the two input sinusoidal signals to have the same amplitude to produce a two-tone mixed signal; if the amplitudes are mismatched, a higher toned signal will be generated. Due to the resulting signal's extreme complexity, it is extremely difficult to extract useful information from either time series analysis or the frequency domain analysis.

With the assumption that the amplitudes of the input sinusoidal signals are very closely matched, equation 2.5 can thus be obtained. To reconstruct a purely sinusoidal signal from the mixed signal that is obtained through the ADC process, it is obvious that the expression given in 2.5 should be divided by one of the two sinusoidal terms in expression 2.5. Equations 2.6 through 2.7 give an example of the division process:

$$\frac{2\sin(\frac{2\pi(f_1+f_2)}{2}t+\frac{\alpha+\beta}{2})\cos(\frac{2\pi(f_1-f_2)}{2}t+\frac{\alpha-\beta}{2})}{\sin(\frac{2\pi(f_1+f_2)}{2}t+\frac{\alpha+\beta}{2})} \qquad (2.6)$$

$$V_{reconstructed} = 2\cos(\frac{2\pi(f_1 - f_2)}{2}t + \frac{\alpha - \beta}{2}) \quad (2.7)$$

At this point, the motivation of the division is very unclear because the process seems meaningless from a purely mathematical standpoint. However, if the sets of equations are put into real application testing scenarios, they will become very meaningful. Figure 2.3 shows the mathematical representation of the additive summing mixer and the summary of the mathematical expression of the model.

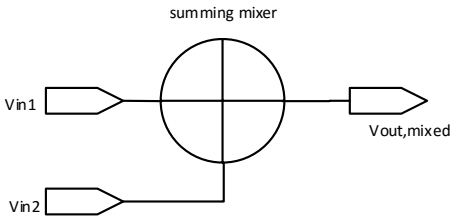

$$V_{in1} = A_1 \sin(2\pi f_1 t + \alpha)$$
$$V_{in2} = A_2 \sin(2\pi f_2 t + \beta)$$
$$V_{out,mixed} = 2\sin(\frac{2\pi(f_1 + f_2)}{2}t + (\frac{\alpha + \beta}{2})) \times \cos(\frac{2\pi(f_1 - f_2)}{2}t + (\frac{\alpha - \beta}{2}))$$

Figure 2.3: Additive summing mixer mathematical model

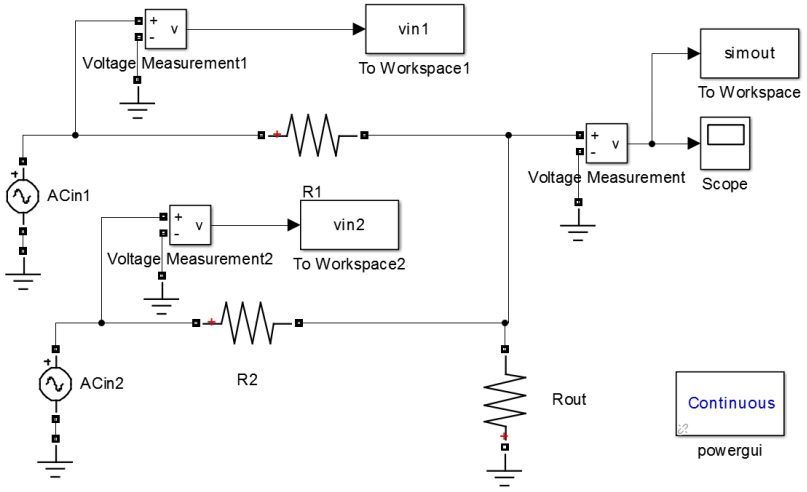

Figure 2.4: Additive summing mixer simulink circuit simulation

Figure 2.4 is the MATLAB Simulink circuit model that represents the mathematical model shown in figure 2.3. The Simulink circuit model with the signal parameter shown in figure 2.5 is used to demonstrate the effects of amplitude and phase mismatch between input signals prior to entering the mixer on the reconstructed signal when the mixed signal is divided by an uncorrected division signal. Figure 2.7 shows a more general parameter setup where the proper dividing signal Sig_{divide} is accounted for. In the circuit model, the resistors R_1 and R_2 are chosen to be the same value so the two half circuit branches are perfectly balanced.

$$\alpha = 0, \beta = [0, 30^o]$$
$$A_1 = 1, A_2 = [1, 1.5]$$
$$f_1 = 30Hz,\ f_2 = 60Hz$$
$$\text{Sig}_{divide\_1} = \sin(\frac{2\pi(f_1 + f_2)}{2}t)$$

Figure 2.5: Circuit parameter setup 1

The circuit parameters shown in figure 2.5 are used in setup 1. In setup 1, 4 combinations formed by the phase shift β and amplitude A_2 are used for signal V_{in2}. After mixing, the output signal from the mixer $V_{out,mixed}$ is divided by an uncorrected reconstruction sinusoidal signal Sig_{divide_1}. The resulting waveforms are shown in figure 2.6.

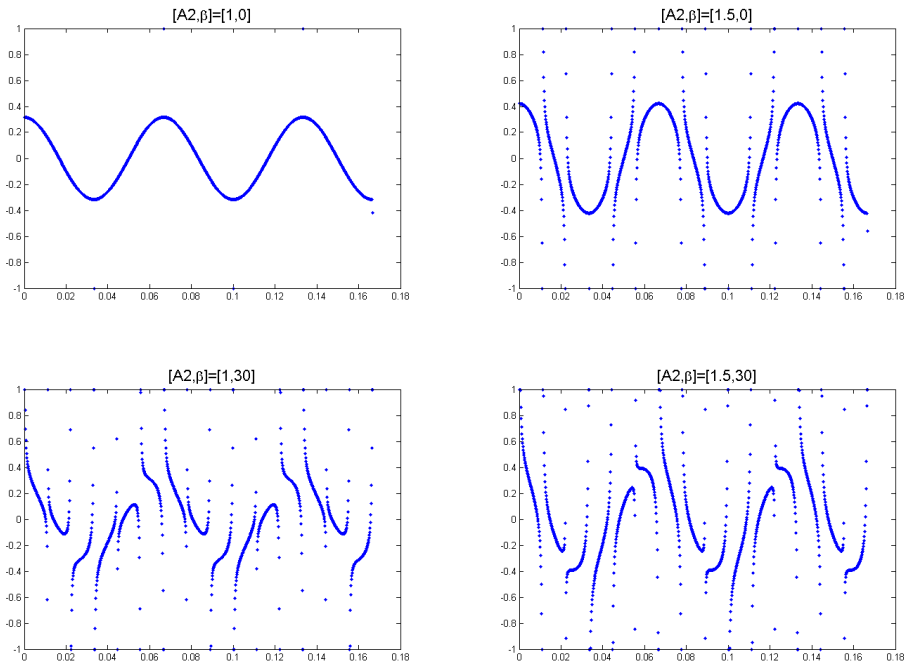

Figure 2.6: $V_{out,mixed}/Sig_{divide\_1}$

As shown in figure 2.6, the only configuration of Sig_{divide} to produce a perfect pure tone sinusoidal signal is when input sinusoidal signals have matched amplitudes and the phase shift of Sig_{divide} corrected to account for the phase difference in the incoming signals.

As mentioned before in section 2.1, it is important for the incoming sinusoidal signals to have matching amplitudes in order to create a $V_{out,mixed}$ with only two frequency components f_1+f_2 and f_1-f_2. Setup 2 makes the assumption that the amplitudes of input signals are perfectly matched; instead, setup 2 will focus on the effectiveness of accounting for the phase shift in Sig_{divide_2} in order to recover a perfect pure tone sinusoidal signal. The circuit parameter of setup 2 is shown in figure 2.7.

$$\alpha = 20^o, \beta = 30^o$$
$$A_1 = 1, A_2 = 1$$
$$f_1 = 30Hz,\ f_2 = 60Hz$$
$$\text{Sig}_{divide,uncorrected} = \sin(\frac{2\pi(f_1 + f_2)}{2}t)$$
$$\text{Sig}_{divide,corrected} = \sin(\frac{2\pi(f_1 + f_2)}{2}t + \frac{\alpha + \beta}{2})$$

Figure 2.7: Circuit parameter setup 2

In the second simulation setup shown in figure 2.7, the input signals are perfectly amplitude matched; the phase shifts between the two signals are chosen to be 20 and 30 degrees for V_{in1} and V_{in2} so that the phase shift condition is more generic. Comparing the output generated by an uncorrected and a corrected Sig_{divide} shown in figure 2.8, it is evident that it is possible to reconstruct a pure sinusoidal wave when the phase shift between the incoming signals is accounted for.

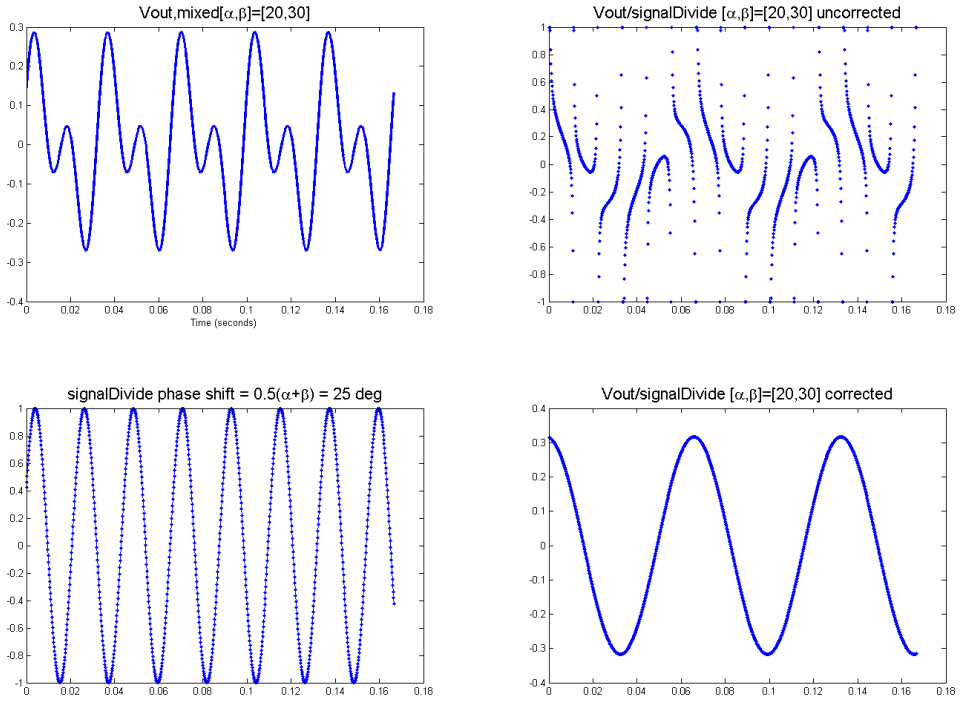

Figure 2.8: $V_{out,mixed}/Sig_{divide\_2}$

The important mathematical property behind the additive summing mixer and the process of reconstructing the sinusoidal wave from the mixed signal are the enablers behind the technique to implement the acoustic impedance sensing platform on the smartphone.

2.4 Phase Delayed Summing Mixer

In sections 2.2 and 2.3, the phase delay between the incoming signals are generated in simulation through controlling the phase difference between the input signals. This is possible in simulation to demonstrate the mathematical principle behind the summing mixer; however, in real application of the acoustic impedance sensing platform, the phase difference is generated through the circuit when the input signals pass through complex DUTs (device-under-test). The circuit used to construct the additive summing mixer is shown in figure 2.9. The impedance measurement circuit shown in figure 2.9 is similar to the model presented in figure 2.4: A pair of stereo input signals are generated and a mixed output $V_{out,mixed}$ is captured at the output of the circuit. The only difference between the two circuits is the way that the phase shift between two inputs is generated. The mathematical modeling and application of the circuit will be discussed in chapter 4.

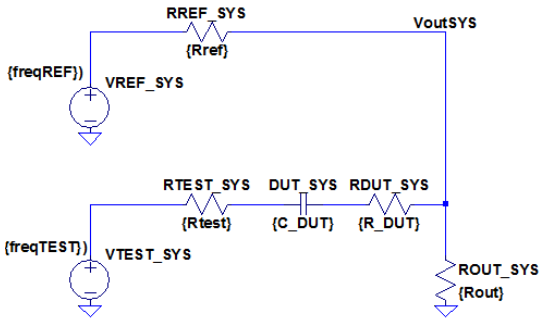

Figure 2.9: Additive summing mixer for acoustic impedance measurement

CHAPTER 3:

SMARTPHONE AUDIO PERFORMANCE CHARACTERIZATIONS

In chapter 2, it is shown that it is feasible to perform sinusoidal signal reconstruction in the additive summing mixer when the amplitudes of the input signals are perfectly matched. Chapter 3 will be dedicated to discussing the feasibility of using a smartphone as a test fixture platform for the acoustic impedance sensing application.

To characterize the smartphone's capability for the impedance sensing application, the device's acoustic performance parameters are thoroughly examined. The acoustic performances include: frequency response, input output voltage linearity, and output voltage vs. reference resistance. Ultimately, when all of the measurements are combined, it is possible to generate an adequate approximation circuit model to model the system's output impedance characteristics. In the smartphone test fixture setup, the system's output impedance is the smartphone microphone channel's input impedance.

The smartphone used in the test setup is the Google Nexus 4 Android smartphone manufactured by LG. In addition to the smartphone, an Agilent 33120A function generator and a National Instruments USB-4065 programmable multimeter are used for multi-point parametrized sweep and data acquisition. In the frequency response test, both instruments are controlled using National Instruments LabVIEW software.

3.1 Output vs. Input Voltage Linearity

The first and the most fundamental characterization is the output vs input voltage linearity test; a schematic of the test setup is shown in figure 3.1. In the output vs. input voltage linearity test, the input voltage amplitude is incrementally adjusted from 0 to 1 V with the step size of 50 mV. This linearity test is also repeated for five different frequencies: 20 Hz, 30 Hz, 1 kHz, 2 kHz and 10 kHz. The output vs. input voltage sweep plot is shown in figure 3.2.

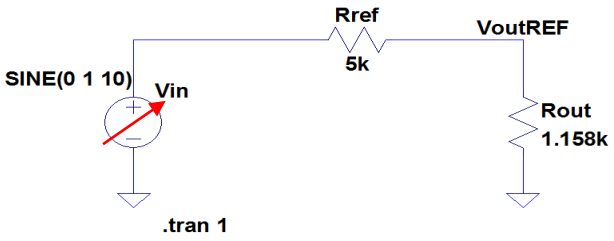

Figure 3.1: Output vs. input voltage linearity circuit setup

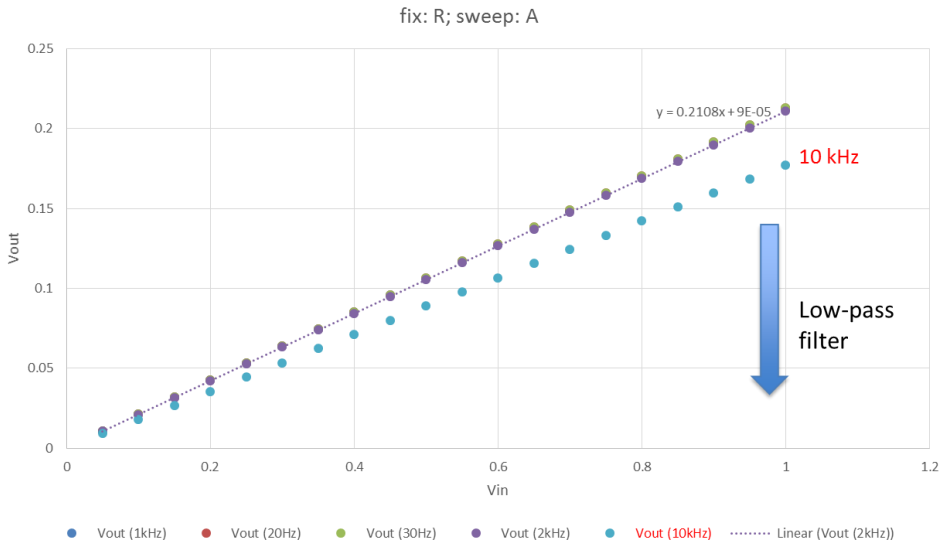

Figure 3.2: Output vs. input voltage linearity plot

The output vs. input voltage linearity plots gathered for all frequencies are almost the same except for the case of 10 kHz. Although the plot is still very linear, the amplitude measured at the system output is significantly lower than that measured at the lower frequencies. This behavior is expected of a commercial smartphone because it is reasonable to limit the audio frequency range to the human audible range which is usually between 10 Hz and 10 kHz. The observed signal attenuation is very possibly the effect caused by a hardware low-pass filter. The behavior of the low-pass filter will be observed again in the frequency response analysis in section 3.3.

From the low frequency plots, it is also possible to estimate the system output resistance value assuming the microphone input impedance is purely resistive at low frequencies. The estimated R_{out} is calculated to be 1.158 kΩ based on the slope of the best-fit line on the 2 kHz dataset.

3.2 Output Voltage vs. Reference Resistance

The output voltage vs. reference resistance linearity test simulates a simple resistance measurement situation; the test circuit setup is shown in figure 3.3. The reference resistance value R_{ref} is swept from 2 kΩ to 50 kΩ. The resulting output voltage vs. reference resistance plots is shown in figure 3.4. Since it has been established in section 3.1 that the system output has a low-pass filtering effect, the test frequency in the reference resistance linearity test is pushed to 100 kHz. In the setup, a total of four different frequencies are tested: 330 Hz, 1 kHz, 10 kHz and 100 kHz.

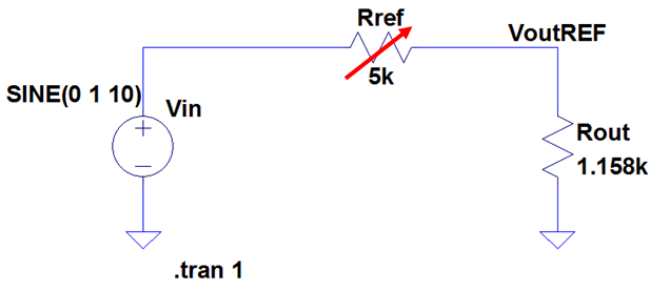

Figure 3.3: Output voltage vs. reference resistance circuit setup

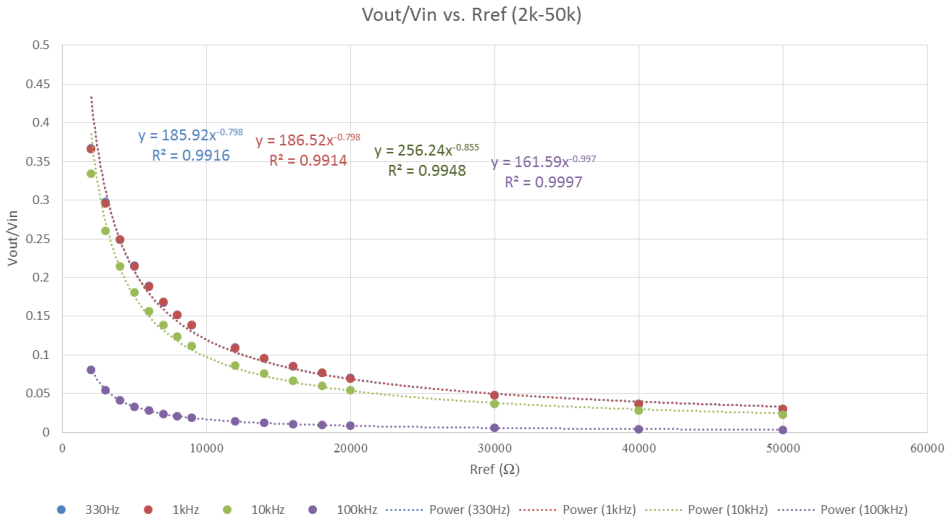

Figure 3.4: Output voltage vs. reference resistance plot

The shape of the R_{ref} test exhibits the expected "1/x" shape of a pure resistor divider circuit when the variable resistance is in the denominator; the mathematical expression of the divider circuit is shown in equation 3.1. Also as expected, the low-pass filtering effect is apparent when the test is run at 100 kHz frequency; the output voltage is heavily suppressed at higher frequencies. In order to find the maximum range of operating frequencies, it is necessary to conduct a frequency response test of the microphone

channel so the impedance measurement range can be maximized or appropriately compensated.

$$\frac{V_{out}}{V_{in}} = \frac{R_{out}}{R_{out} + R_{ref}} \tag{3.1}$$

3.3 Frequency Response

The frequency response test is conducted using a LabVIEW controlled instrument setup, the front panel of which is shown in figure 3.5. The program steps frequency values from start frequency to stop frequency with the specified resolution steps. After each step of the frequency sweep, an AC voltage measurement is taken by the NI DMM. In order to find the cutoff frequency as accurately as possible, a total of 500 frequency steps are taken from 20 Hz to 100 kHz. The amplitude of the sinusoidal signal generated is lowered to 0.2 V to protect the microphone circuitry due to the length of the frequency response test (roughly 10 hours). The circuit setup and the frequency response plot are shown in figure 3.6 and 3.7.

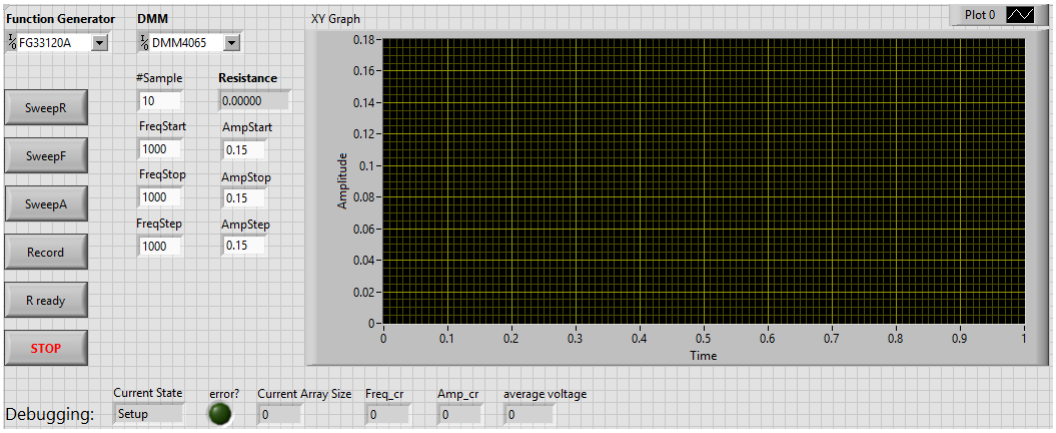

Figure 3.5: LabVIEW front panel for smartphone calibration

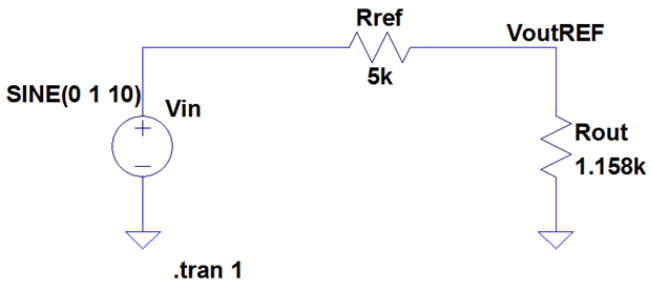

Figure 3.6: Frequency response test circuit setup

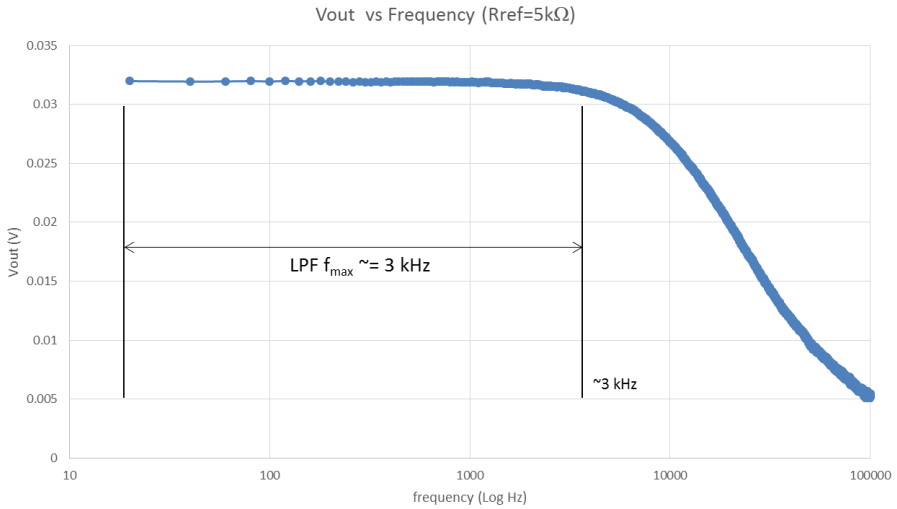

Figure 3.7: Frequency response plot

With a reasonably good number of test points as shown in figure 3.7, the response resembles a classic low-pass filter with a 3 dB frequency at around 5 kHz. In the impedance measurement application, the frequency of interest is more conservative than the 3 dB point. An operating range of 3 kHz is selected because the frequency response is almost flat from 20 Hz to 3 kHz.

3.4 Modeling Unknown Microphone Input Resistance

As shown in sections 3.1 – 3.3, the smartphone microphone input channel is designed to filter out high frequency signals that are beyond the human hearing range (> 10 kHz). For all three tests, the simple voltage divider model has been assumed. If it is desired for the microphone channel to be modeled precisely, the circuit model shown in figure 3.8 can be used. However, for the impedance measurement application discussed in chapter 4, it is adequate to utilize the simple circuit model shown in figure 3.9 as long as the operating frequency is limited to below 3 kHz. At frequencies under 3 kHz, the microphone output impedance behaves very close to purely resistive.

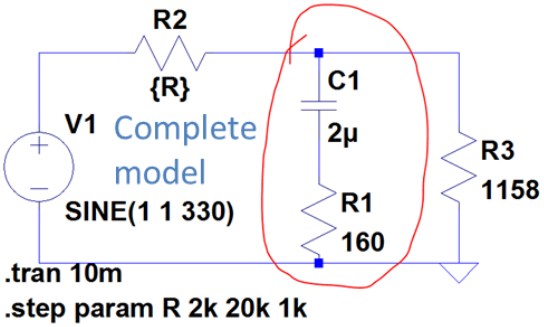

Figure 3.8: Mic input full model

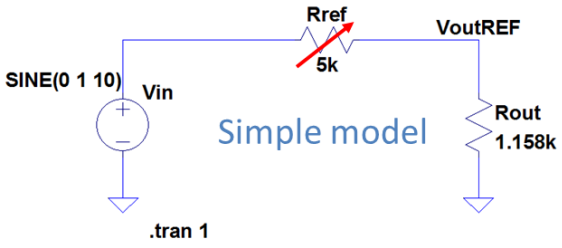

Figure 3.9: Mic input low-frequency model

3.5 Determining Unknown Microphone Input Resistance

Leveraging the simple circuit model presented in figure 3.8, it is possible to obtain a good estimate of the microphone input resistance denoted as R_{out} through calibration. It is critical to perform the calibration in a real application due to the changes in the resistance values from device to device. The deviation can be substantial even on the same modeled smartphones. The calibration process is similar to the linearity test done in section 3.1.

CHAPTER 4:

IMPEDANCE DETECTION ALGORITHM

The mathematical and platform validations were performed in chapter 2 and chapter 3. In chapter 4, the mixer circuit architecture is proposed and validated. The circuit architecture shown in figure 2.9 is reiterated in figure 4.1. The circuit shown in figure 4.1 is a good representation of the additive summing mixer mathematical model shown in figure 2.3; this can be validated through performing the circuit superposition analysis on the mixer circuit in section 4.1.

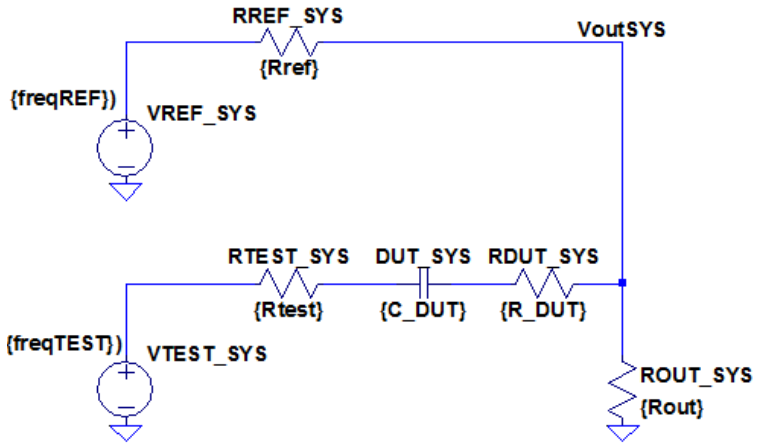

Figure 4.1: Additive summing mixer for acoustic impedance measurement

4.1 Superposition Circuit Modeling

The additive summing mixer circuit shown in figure 4.1 can be decomposed into two branches through the Thevenin circuit superposition theory. The superposition equivalent circuits of figure 4.1 are shown in figure 4.2.

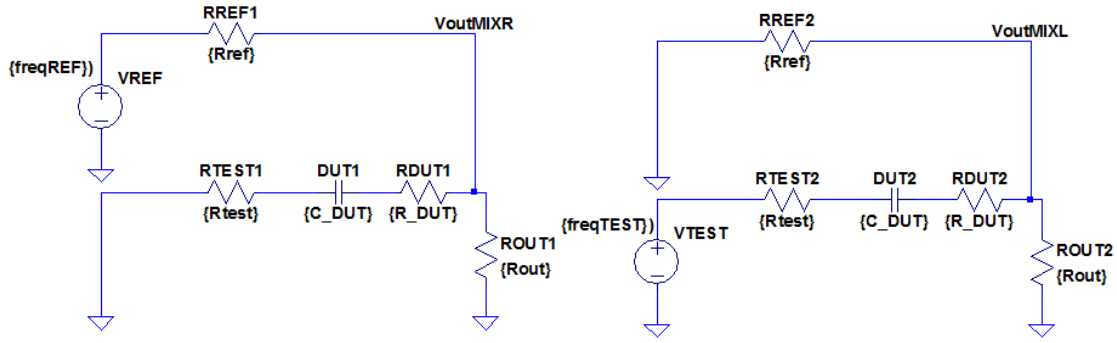

Figure 4.2: Superposition circuits of the additive summing mixer circuit

"The superposition theorem for electrical circuit states that for a linear system the response (voltage or current) in any branch of a bilateral linear circuit having more than one independent source equals the algebraic sum of the responses caused by each independent source acting alone, where all the other independent sources are replaced by their internal impedances" [14]. For the additive summing mixer circuit shown in figure 4.1, the superposition equivalent circuits shown in figure 4.2 are generated by suppressing one voltage source at a time and adding the nodes of interest together to reconstruct the original circuit's behavior. In figures 4.1 and 4.2, each voltage source represents a single stereo audio channel that is also a part of the 3.5 mm headphone jack.

The superposition equivalent models are simulated and compared to the full mixer circuit model with real DUT test scenarios to replicate a real testing environment. Figure 4.3

shows the full additive summing mixer circuit with circuit simulation parameters. Figure 4.4 compares the transient analysis on the voltage directly measured from the mixer $V_{out,sys}$ with the sum of output voltages $V_{out,mixR}$ and $V_{out,mixL}$ from the circuit in figure 4.2. From the plot in figure 4.4, the two waveforms perfectly match, hence proving the validity of the superposition circuit analysis on the additive summing mixer.

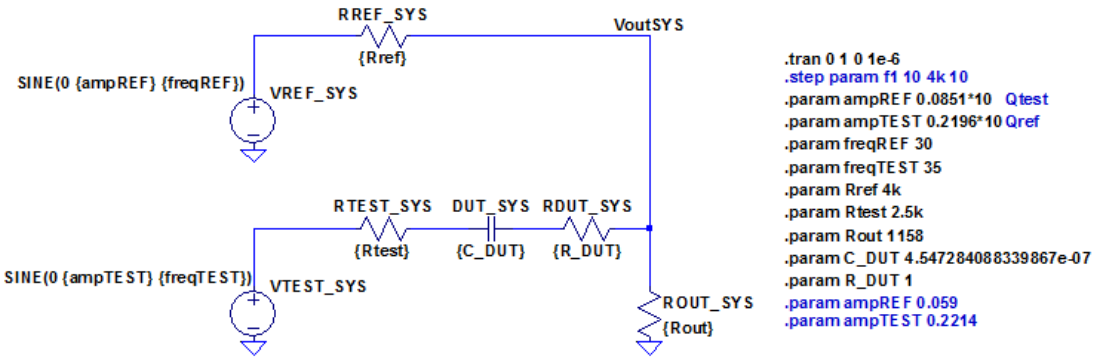

Figure 4.3: Additive summing mixer circuit with simulation parameters

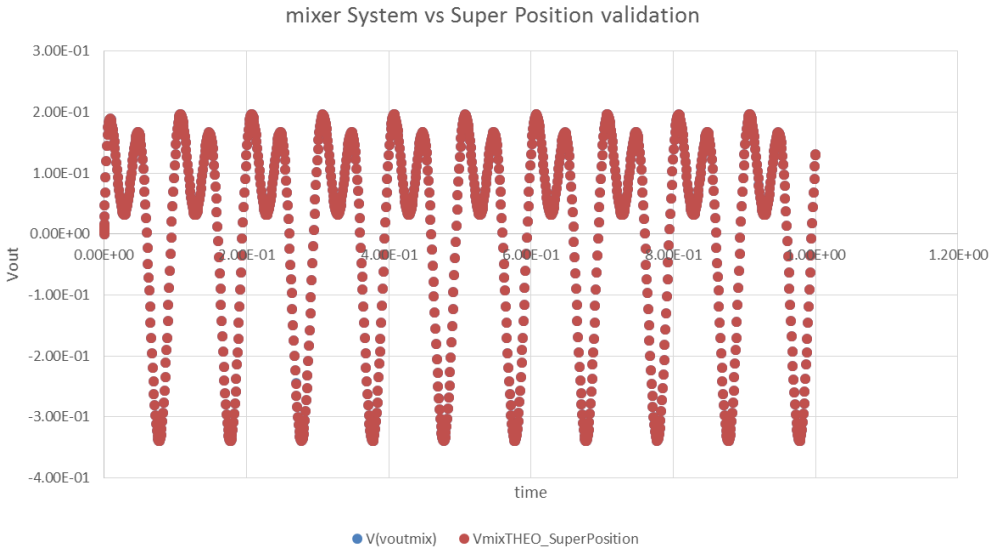

Figure 4.4: Superposition vs. direct mixer output voltage comparison

4.2 Impedance Response and Look-Up Table

Since the theory of superposition is proven to be valid in simulation, the next step is to break down the complex mixer circuit into the two superposition equivalent circuits with single voltage source shown in figure 4.5 for mathematical circuit analysis. By the principle of superposition, the total mixer output signal can be expressed as the sum of output signals produced by each superposition half-circuit.

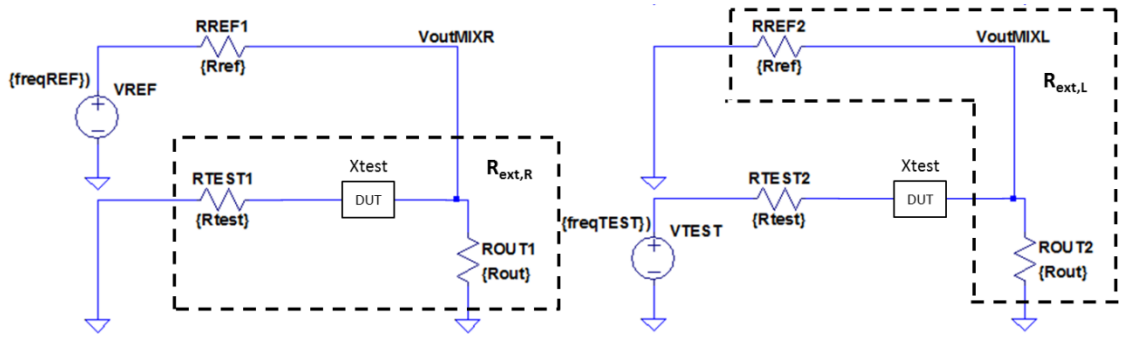

Figure 4.5: Superposition circuits mathematical analysis

The mathematical expression for finding $V_{outMIX,R}$ is simply the voltage divider between the output impedance $R_{ext,R}$ and the reference resistor $R_{ref:}$

$$Q_R = \frac{V_{out,R}}{V_{in,REF}} = \frac{R_{ext,R}}{R_{ext,R} + R_{in} + R_{ref}} \tag{4.1}$$

where the expression of $R_{ext,R}$ is:

$$R_{ext,R} = \frac{R_{out} X_{test} + R_{out}(R_{test} + R_{in})}{R_{test} + R_{in} + R_{out} + X_{test,REF}}, X_{test,REF}(f_{REF}) \tag{4.2}$$

Similarly for the right channel half-circuit, the $V_{outMIX,L}$ can also be expressed using voltage divider between $R_{test,}$ X_{test} and $R_{ext,}$:

$$Q_L = \frac{V_{out,\mathrm{L}}}{V_{in,\mathrm{TEST}}} = \frac{R_{ext,\mathrm{L}}}{R_{ext,\mathrm{L}} + R_{in} + R_{test} + X_{test}}, X_{test}(f_{test}) \tag{4.3}$$

where $R_{ext,L}$ can be expressed as:

$$R_{ext,\mathrm{L}} = \frac{R_{out}(R_{ref} + R_{in})}{R_{ref} + R_{in} + R_{out}} \tag{4.4}$$

In both the reference channel and test channel, resistance R_{in} is a built-in stereo output resistance of 20 Ω; this resistance can be ignored in calculations.

In each half-circuit, the only unknown variable is the impedance of the DUT X_{test}. Assuming X_{test} is purely reactive with only imaginary component of the impedance, X_{test} can be expressed as equation 4.5, where $\Omega_{DUT} > 0$ when DUT is net inductive and $\Omega_{DUT} < 0$ when DUT is net capacitive. The sign of Ω_{DUT} does not affect the amplitude of the output voltages, but it does affect the phase shift of the output voltages. With the above assumption, each half-circuit mathematical expression reduces down to a single variable one-to-one function; hence, two sets of output voltage magnitude and phase look-up-tables based on the impedance value Ω_{DUT} can be generated for each half-circuit as shown in figure 4.6.

$$X_{test} = j\Omega_{DUT} \tag{4.5}$$

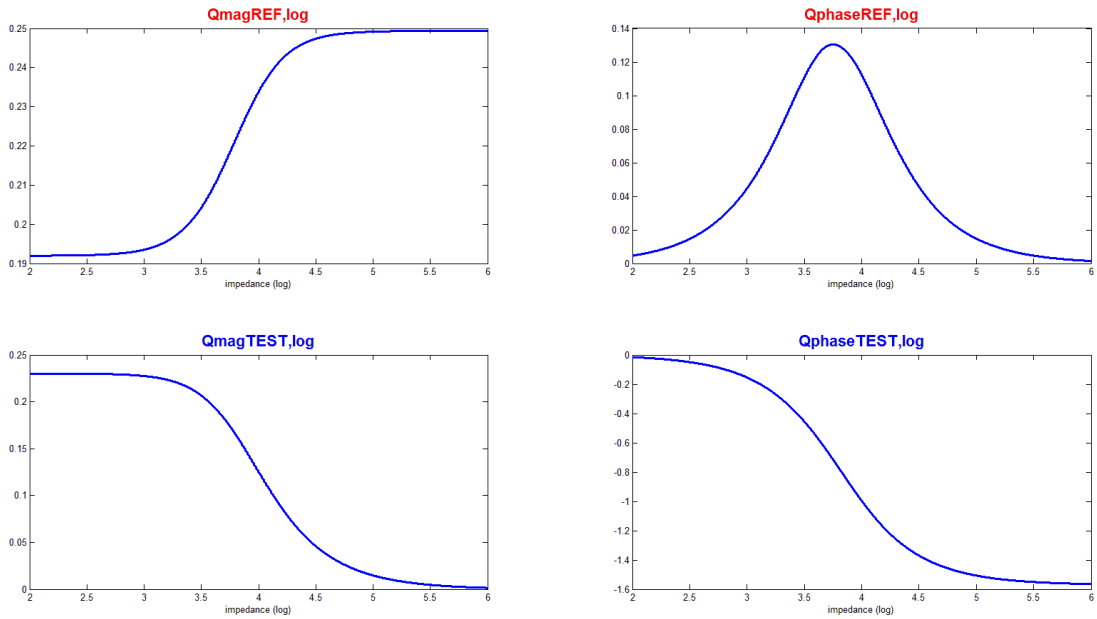

Figure 4.6: Output voltage magnitude and phase look-up-table plots

With the look-up-tables for each half-circuit channel, it is very easy to match the input signal amplitudes as emphasized heavily in chapter 3 because of its importance for eliminating higher order sinusoidal components in the mixed output signal. Since the input frequencies from each stereo channel are known and controlled by software, and the impedance of the DUT is directly proportional to the frequency in the Z domain, to produce the pair of signals going into the mixer that have equal magnitude is a simple matter of changing the stereo input signal amplitudes according to the ratio found through the LUT.

Start with both stereo output channels producing signals with the same amplitude V_m, and a hypothetical point on the reference channel V_{out}/V_{in} LUT $Q_{mag,REF}$ corresponding to a

impedance value of roughly $Z_{DUT,REF}$. With the impedance found on the reference channel, the impedance of the same DUT seen by the test channel is:

$$Z_{DUT,TEST} = Z_{DUT,REF} \frac{f_{TEST}}{f_{REF}} \tag{4.6}$$

With the impedance value seen by the test channel $Z_{DUT,TEST}$, the V_{out}/V_{in} response of the test channel can be found on the $Q_{mag,TEST}$ plot. With the V_{out}/V_{in} ratios obtained for both the reference and test channels, the amplitudes generated by the stereo channels can be found using equation 4.7. The pair of amplitudes found by 4.7 will ensure that the immediate incoming signals for the additive summing mixer have the same amplitude, thus satisfying the amplitude matching rule.

$$V_{REF} = V_m \frac{Q_{mag,\mathrm{TEST}}}{Q_{mag,REF}},\ V_{TEST} = V_m \frac{Q_{mag,REF}}{Q_{mag,\mathrm{TEST}}} \tag{4.7}$$

At this point, it is assumed that the V_{out}/V_{in} plot for either of the two channels is known, but in fact, it is impossible to obtain a direct measurement of the V_{out}/V_{in} on either channel because the summing mixer cannot be broken into the two physical circuits shown in figure 4.5. To bridge simulation and reality, a third LUT from the circuit shown in figure 4.7 is needed. The circuit equivalent shown in figure 4.7 can be physically obtained by turning off the reference channel to form a true mono configuration.

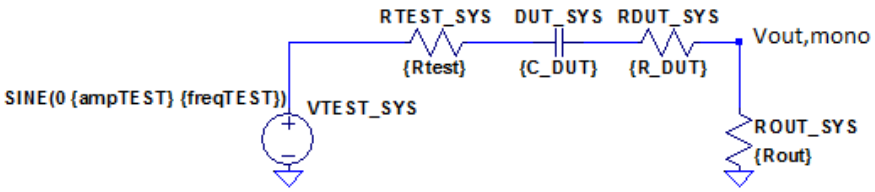

Figure 4.7: One branch test circuit

The V_{out}/V_{in} response of the circuit shown in 4.2.3 can be expressed by a simple voltage divider equation:

$$Q_{mono} = \frac{V_{out,mono}}{V_{in,test}} = \frac{R_{out}}{R_{test} + R_{out} + X_{test}}, X_{test}(f_{test}) \tag{4.8}$$

Equation 4.8 greatly resembles the half-circuit equation for the test channel shown in equation 4.4. A LUT similar to that shown in figure 4.6 can be also generated for the one branch test circuit by sweeping the DUT impedance value. The one-branch LUT plot is shown in figure 4.8.

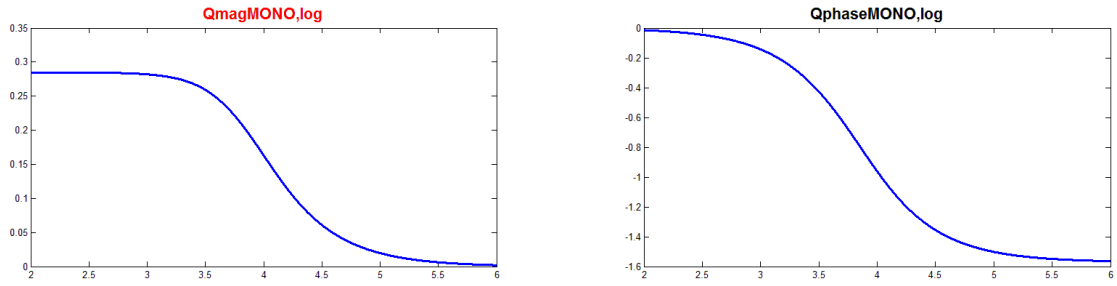

Figure 4.8: One branch test circuit LUT

Comparing the Q plots for mono (figure 4.8) and test channel (figure 4.6) setups, the magnitude and phase responses follow very similar shapes as expected. Figure 4.9 shows

an overlapped comparison of mono and test magnitude and phase response LUTs. When test channel magnitude and phase LUTs are normalized to fit the mono LUTs, the two LUTs exhibit very similar shape. By using the mono sweep on the test channel, voltage response can be physically measured. Through the amplitude matching techniques shown in equations 4.6 and 4.7, the V_{out}/V_{in} response on the test channel in the full mixer circuit can be deduced from the measurements done on mono; then the V_{out}/V_{in} response can be further deduced for the reference channel in the full mixer circuit.

Figure 4.10 shows a summary of all three LUTs that will be used for the impedance detecting algorithm discussed in section 4.3.

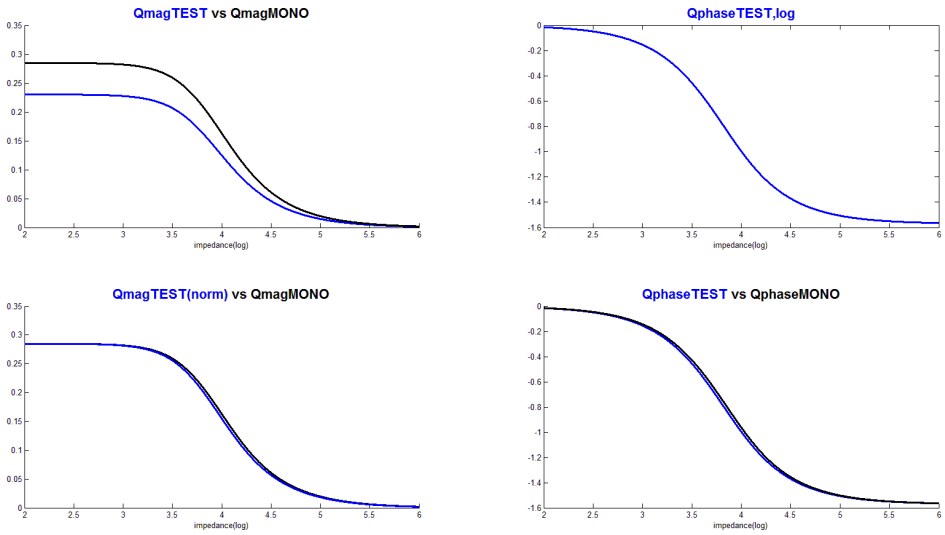

Figure 4.9: Mono, test LUT comparisons

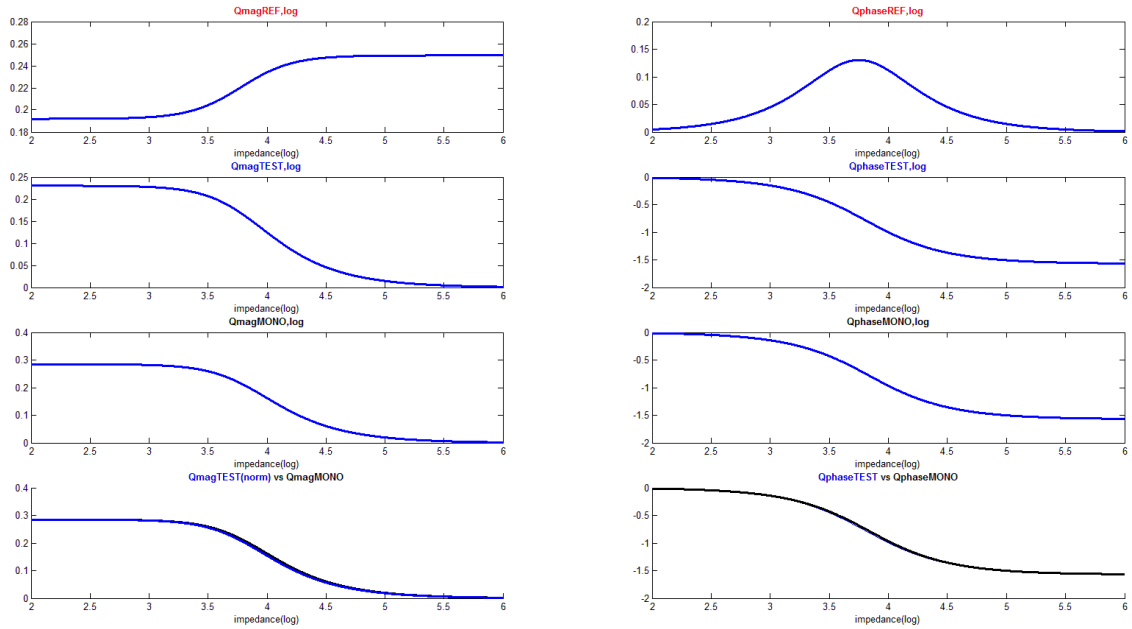

Figure 4.10: REF, TEST, mono LUT summary

4.3 Unknown Impedance Detection: Algorithm Overview

There are four main steps involved in the additive summing mixer based impedance measurement algorithm:

1. Characterize device microphone input resistance R_{out} (section 3.5).

2. Generate look-up tables for mixer half circuits and mono test circuit (section 4.2).

3. Perform frequency sweep on mono channel to obtain a suitable point on mono LUT and calculate LCR.

4. Find amplitude and phase shift for mixer superposition circuits, and derive the

reconstruction waveform to check results (section 2.3).

Steps 1 and 2 will be briefly summarized as these were topics discussed in previous chapters. It is necessary to characterize each smartphone device without DUT attached as step 1 because the microphone input impedance R_{out} is a critical component in the LUT generation done in step 2. The mic impedance can be found by the methods described in section 3.5. After R_{out} is available, step 2 is purely based on circuit model and mathematics. With all the resistive elements either provided by the user or determined in step 1, the only unknown variable in the circuit model is the DUT impedance, so the impedance value is used to generate the V_{out} amplitude and phase LUTs for the three aforementioned circuit setups shown in section 4.2.

Step 3 is the most important step in the entire algorithm and involves iterating through different frequencies to narrow down on the frequency that will obtain an optimal DUT impedance point on the mono LUT shown in figure 4.8. Provided an unknown DUT that is either capacitive or inductive, the DUT's impedance can be controlled by adjusting the input sinusoidal signal frequency. Also, through the frequency spectroscopy analysis, the DUT's electrical characteristics can be obtained. Taking the mono test circuit setup shown in figure 4.7 as an example, if the DUT is net capacitive, the output voltage will be positively related to input signal frequency because the impedance of capacitive devices is inversely related to incident frequency; the opposite is true for inductive devices, and if the frequency response is flat, then the DUT can be modeled as a purely resistive device. The frequency spectroscopy analysis used in this discussion assumes the frequencies are low enough that resonance is avoided where possible.

As the DUT's net electrical characteristics are determined by the method mentioned above through the technique of frequency spectroscopy, it is then possible to traverse on the mono LUT to find the suitable impedance point on figure 4.11, which is figure 4.8 revisited for convenience. A suitable impedance point is defined as a point on the plot which the sensitivity of impedance measurement $\Delta Q_{mag}/\Delta Z_{DUT}$ is maximized. Tracing through the $Q_{mag,MONO}$ plot shown in figure 4.11, the range for the suitable impedance points can be found in Q_{mag} values between 0.25 and 0.05. To further optimize the test procedure, it is reasonable to select the mid-point between the above ranges; let the point be $Q_{magMono\_target}$ by marked as the red dot on the Q_{mag} LUT in figure 4.11.

As $Q_{mag,Mono\_target}$ is identified, the frequency sweep from $V_{in,Test}$ operated on the mono test circuit is done to find the test channel frequency f_{test} that corresponds to the Z_{DUT} which produces the target voltage response. Taking an inductive DUT device as an example, to narrow in on the target response, if the Q measured is larger than Q_{target} (on the left of the LUT curve), then the frequency needs to be increased to move more to the right to approach Q_{target}. The opposite is true for a capacitive device and one example evaluation testbench will be shown in section 4.4 with a random capacitance value.

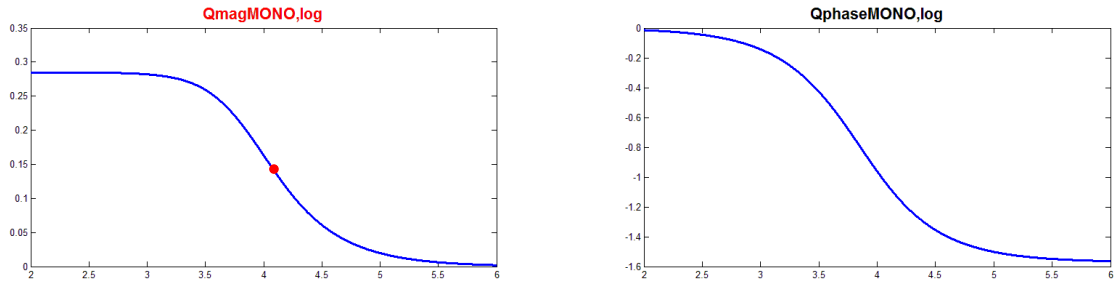

Figure 4.11: One branch test circuit LUT

After the target impedance frequency pair has been acquired, it is possible to back-calculate the capacitance or inductance value at this point if the device is purely imaginary with no real component. It is always necessary to use the additive summing mixer signal reconstruction technique to check the impedance results obtained through the mono test. Also, for complex impedance systems with real and imaginary components, it is very difficult to accurately characterize the system with mono-only test setup.

To test the impedance result obtained through the mono test using the full additive summing mixer, appropriate amplitudes and phases for both reference and test channels are needed for the reconstruction equation. As mentioned in section 4.2 and seen in equation 4.7, the voltages are simply the ratios of Q_{mag} found for each channel through LUT process initialized by the Mono LUT as described in section 4.2. The expression for the reconstruction equation is shown in equation 4.9 which is a reiterated version of $Sig_{divide,corrected}$ shown in figure 2.5 where p_{ref} and p_{test} can both be looked up from each half-circuit LUT:

$$Sig_{divide} = \sin(2\pi \frac{f_{ref} + f_{test}}{2} t - \frac{p_{ref} + p_{test}}{2}) \tag{4.9}$$

If the corrected signal generated by dividing the mixed signal by Sig_{divide} is very close to a pure tone sinusoidal signal, then the impedance measurement is successful. Section 4.4 will provide an example of a simulated measurement procedure.

4.4 Unknown Impedance Detection: An Example

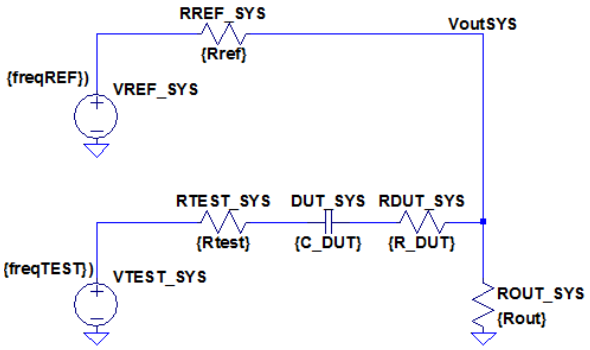

$$R_{ref} = 6\ k\Omega$$
$$R_{test} = 5\ k\Omega$$
$$R_{out} = 2\ k\Omega$$
$$R_{DUT} = 0$$
$$C_{DUT} = 25.843\ nF$$

Figure 4.12: Additive summing mixer testbench circuit with parameters

Figure 4.12 shows the test bench circuit used by the impedance measurement testbench simulation. The capacitance value is randomly generated within a set range. Following the algorithm procedure described in section 4.3 and assuming that steps 1 and 2 are already done (LUTs available), this example will start with step 3, the mono channel frequency sweep to find the desired $Q_{mag,mono}$ value and the corresponding impedance value.

The frequency sweep range is set to between 100 Hz and 3 kHz. The control algorithm keeps changing the mono frequency until $Q_{mag,test}$ is within 0.1% of $Q_{mag,target,}$ which is chosen to be 0.15. Figure 4.13 shows the control steps taken by the algorithm to reach the 0.1% range, the frequency settled at 543 Hz.

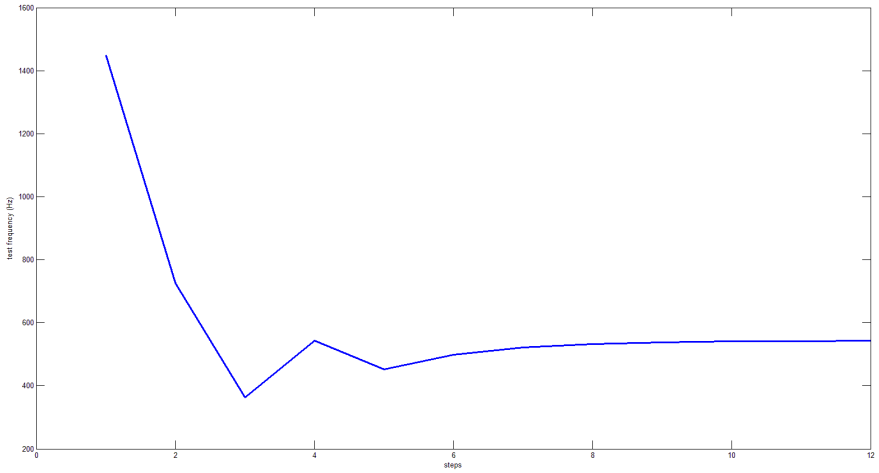

Figure 4.13: Frequency vs. control step for mono frequency sweep

After using the LUTs generated for the superposition half circuits, f_{ref}, f_{test}, P_{ref} and P_{test} are found and tabulated in figure 4.14. Figure 4.15 shows the signal produced measured at the output of the mixer. Figure 4.16 shows the reconstructed signal with close resemblance to a pure tone sinusoidal signal. With the reconstructed signal being sinusoidal as the primary indication of successful measurement, in addition, the capacitance value that is calculated from the algorithm is 25.827 nF, very close to the actual device capacitance of 25.843 nF.

$f_{ref} = 452.54$ Hz $\qquad P_{ref} = 0.0934$ rad

$f_{test} = 543.04$ Hz $\qquad P_{test} = -1.0492$ rad

Figure 4.14: Summary of input signal properties

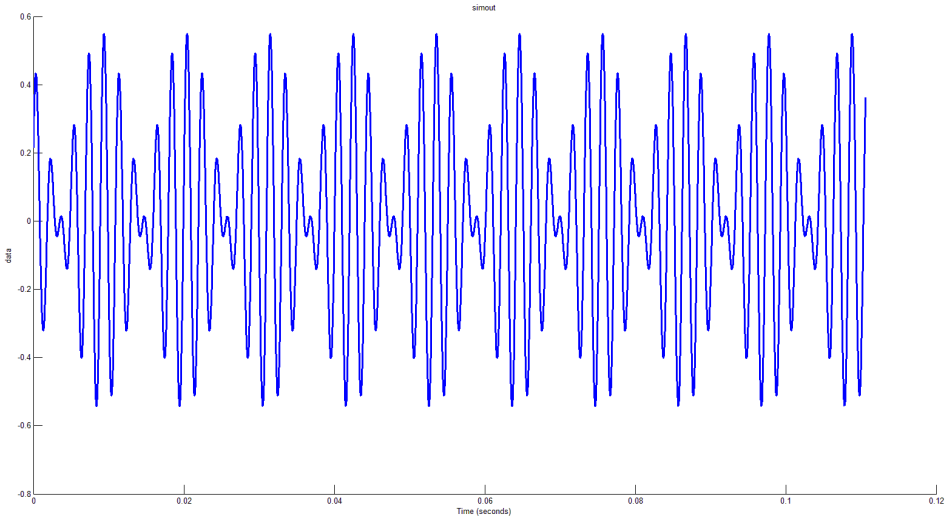

Figure 4.15: Voltage output from mixer $V_{out,mixed}$

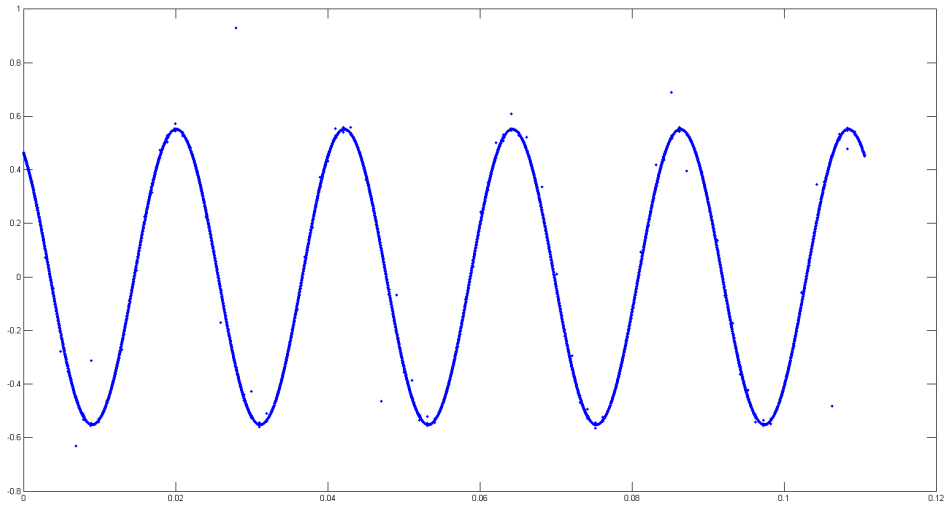

Figure 4.16: Reconstructed signal after division

CHAPTER 5:

SUMMARY AND FUTURE WORK

The additive summing mixer based impedance measurement method presented in this work is able to accurately characterize the DUT's device characteristics. The smartphone based summing mixer method is advantageous because the circuit is purely dependent on the stereo signals generated by the smartphone's audio jack, thus making the circuit battery-less.

In addition to the smartphone focused implementation presented in this paper, the mixer based impedance measurement method can be very flexibly implemented on any system with stereo signal generation and mono reception because the method presented is purely mathematical.

For future work, the impedance measurement functionality of the software needs to be expanded so the system can measure more complex impedance systems that contain DUTs with both real and imaginary impedance components. Also, the smartphone's internet capability can be leveraged so that the impedance measurement can be implemented for medical sensing and diagnosis such as breast cancer self-diagnosis.

REFERENCES

[1] Wikipedia, "Electrical impedance," https://en.wikipedia.org/wiki/Electrical_impedance.

[2] O. Heaviside, in *Electrical Papers*, The Electrician Printing and Publishing Co, 1886, p. 212.

[3] H. Schwan, "Electrical properties of body tissues and impedance plethysmography," *IRE Transactions on Medical Electronics*, Vols. PGME-3, no. 1955, pp. 32 - 46, 1955.

[4] W. Tong and W. W. Tang, "Measuring impedance in congestive heart failure: Current," *Am Heart*, vol. 157, no. 3, pp. 402-411, 2009.

[5] M. Elgendi, "On the analysis of fingertip photoplethysmogram signals," *Current Cardiology Reviews*, vol. 8, no. 1, 2012.

[6] P. Shaltis, A. Reisner and H. Asada, "Calibration of the Photoplethysmogram to Arterial Blood Pressure: Capabilities and Limitations for Continuous Pressure Monitoring," in *Engineering in Medicine and Biology 27th Annual Conference*, Shanghai, China, 2005.

[7] *Agilent Impedance Measurement Handbook*, 4th Edition, Santa Clara, CA: Agilent Technologies, 2013.

[8] Analog Devices, "1 MSPS, 12-bit impedance converter, network analyzer," AD5933 datasheet, Sept 2005 [Revised May. 2013].

[9] Y.-S. Kuo, T. Schmid and P. Dutta, "Hijacking power and bandwidth from the mobile phone's audio interface," in *International Symposium on Low Power Electronics and Design*, 2010.

[10] M. Klaper and H. Mathis, "2-Pound RLC meter impedance measurement using a sound card," *elektor*, June 2008.

[11] S. Haykin and B. Widrow, *Least-Mean-Square Adaptive Filters*, Hoboken, NJ, USA: John Wiley & Sons, Inc, 2003.

[12] Analog Devices, *Linear Circuit Design Handbook*, Norwood, MA: Analog Devices, 2008.

[13] T. Michael, *Audio Engineer's Reference Book, 2nd ed*, Burlington, MA: Focal Press, 2013.

[14] Wikipedia, "Superposition theorem," https://en.wikipedia.org/wiki/Superposition_theorem.